J. Mt. Sci. (2016) 13(5): 906-916 e-mail: jms@imde.ac.cn http://jms.imde.ac.cn
DOI: 10.1007/s11629-015-3796-z

GiT-based structural geologic feature analysis of the southern segment of Longmenshan fault zone for earthquake evidence

YE Cheng-ming[1,2] http://orcid.org/0000-0002-6799-0286; e-mail: rsgis@sina.com

CUI Peng[1] http://orcid.org/0000-0002-3973-5966; e-mail: pengcui@imde.ac.cn

Saied PIRASTEH[3] http://orcid.org/0000-0003-0789-0408; e-mail: s2pirast@uwaterloo.ca

Jonathan LI[3] http://orcid.org/0000-0001-7899-0049; e-mail: junli@uwaterloo.ca

MENG Qingkai[2] http://orcid.org/0000-0002-2019-9702; e-mail: 178919968@qq.com

BI Xiao-jia[4] http://orcid.org/0000-0001-6968-1615; e-mail: 19748146@qq.com

ZHANG Jian-qiang[1] http://orcid.org/0000-0003-3908-1082; e-mail: zhangjianqiang83@163.com

1 Institute of Mountain Hazards and Environment, Chinese Academy of Sciences, Chengdu 610041, China

2 Key Lab. of Earth Exploration and Information Technology of Ministry of Education, Chengdu University of Technology, Chengdu 610059, China

3 Department of Geography and Environmental Management, Faculty of Environment, University of Waterloo, Waterloo, Ontario, Canada N2L 3G1, Canada

4 Chengdu Earthquake Mitigation Bureau, Chengdu 610042, China

Citation: Ye CM, Cui P, Pirasteh S, et al. (2016) GiT-based structural geologic feature analysis of the southern segment of Longmenshan fault zone for earthquake evidence. Journal of Mountain Science 13(5). DOI: 10.1007/s11629-015-3796-z

© Science Press and Institute of Mountain Hazards and Environment, CAS and Springer-Verlag Berlin Heidelberg 2016

Abstract: The Longmenshan fault is a thrust fault which runs along the base of the Longmen Mountains in Sichuan province, southwestern China. The southern segment of the fault had two distinct responses to the M_s 8 Wenchuan and M_s 7 Lushan earthquakes. This study determines characteristics of the structural geology of the Longmenshan fault to evaluate how it influenced the two aforementioned earthquakes. This research was done within a Geo-information Technologies (GiT) environment based on multi-source remote sensing and crustal movement data extracted from the Global Positioning System (GPS). The spatial distribution of the southern segment of the Longmenshan fault zone was comprehensively analyzed to study both earthquakes. The study revealed that the Wenchuan and Lushan earthquakes occurred on two relatively independent faults. In addition, there was a nearly constant-velocity crustal movement zone between the two epicenters that probably had a compressive stress with slow motion. Furthermore, the central fault and a mountain back fault gradually merged from north to south. The Lushan earthquake was not an aftershock of the Wenchuan earthquake. The research showed that fault zones within 30–50 km of State Highway 318 are intensive and complex. In addition, crustal movement velocity decreased rapidly, with a strong multi-directional shear zone. Thus, activity in that zone was likely stronger than in the northern part over the medium to long term.

Keywords: Longmenshan fault zone; Geo-information Technologies (GiT); Remote Sensing (RS); Earthquake; Crustal movement

Received: 1 December 2015
Accepted: 22 February 2016

Introduction

In recent decades, geo-information technologies such as orbital remote sensing devices have increasingly been used for the interpretation and mapping of objects for various applications like structural geology and natural hazards (e.g., earthquakes). In addition, satellite images and digital elevation models (DEMs) are very useful for detection, delineation, and interpretation of geological and structural features (Pirasteh et al. 2008; Pirasteh et al. 2011). Faults, folds, and lineaments interpreted from remotely sensed data are often used as indicators of major fractures near the surface (Ali et al. 2003; Ali et al. 2004; Farrokhnia et al. 2011; Pirasteh and Ali 2005). Use of a Laplacian convolution filter on Enhanced Thematic Mapper (ETM+) Landsat band-4 data enhances the ability to extract structural features. However, integration of data from remote sensing, seismicity, and monitoring of crustal movement from the Global Positioning System (GPS) for structural feature extraction, toward the determination of potential earthquakes, has not been accomplished for the area of the two earthquakes.

Dynamically, the collision between the Indian and Eurasian plates has caused large deformation of the Tibetan Plateau. From 35 Ma B.P., the area has been gradually shaped by crustal thickening and uplift motion rather than crustal shortening and northward motion. The rise of the plateau (Li and Zhou 2006) increased the potential for earthquakes in the region. Tectonically, blocks of the plateau have been gradually extruded along some of the boundary fault zones of Bayan Har block, such as the East Kunlun Fault on the north boundary and Xianshuihe fault on the south boundary. The Longmenshan fault zone (LFZ) is on the eastern boundary of the Bayan Har block. It extends to a south segment and its north segment reaches the Minshan fault zone (Zhang et al. 2011).

In China, the LFZ is complex and researchers have learned much about it from different approaches. Its central segment was the site of the 2008 Wenchuan event. Its southern segment contained the Lushan rupture, and includes the Wenchuan-Maoxian, Beichuan-Yingxiu, Pengxian-Guanxian and Dayi faults, with a series of sub-parallel secondary faults.

Li et al. (2013) studied the Lushan M_S 7.0 earthquake and activity of the southern segment of the LFZ. They analyzed tectonic relationships between the Lushan event and 2008 Wenchuan earthquake. In addition, the rupture history of the southern segment of the LFZ was surveyed by field investigations of active tectonics and paleo-earthquake research. They concluded that activity of the southern segment is much different than that of the central section, and late Quaternary activity has propagated forward to the basin in the east. Li et al. stated that the southern segment becomes wider toward the south, with an increasing number of secondary faults, among which individual faults exhibit much weaker surface activity. This means that this section is not as capable of generating a major earthquake as the central segment.

Longmenshan Mountain is characterized by a Pre-Sinian crystalline complex and is bounded by the Maoxian-Wenchuan-Kangding ductile detachment at the western margin and Yingxiu-Beichuan-Luding ductile thrust at the eastern margin.

The Wenchuan M_s 8.0 megaquake and Lushan M_s 7.0 earthquake occurred on May 12, 2008 and April 20, 2013, respectively. Both were destructive with strong intensity. They battered many homes and caused extensive loss of life (Cui et al. 2008; Ehrlich et al. 2009; Liu et al. 2010; Yi et al. 2013). These two earthquakes were associated with the LFZ which had not experienced a major earthquake > M_s 7.0 in hundreds of years. The main body of the LFZ was not active until the two earthquakes occurred over a five-year span. This event has increased researcher understanding of the fault zone distribution and its mobility. The current consensus on the LFZ is that it has three large fractures: a) The root fracture (Wenchuan-Maoxian counties-Pingwu-Qingchuan) extending west to east; b) the central large fracture (Yingxiu-Beichuan-Guangzhuang, epicenter of the Wenchuan earthquake); c) boundary faults (Dujiangyan-Hanwang, epicenter of the Lushan earthquake).

Many researchers (Yuka et al. 2014; Pei et al. 2014) have studied earthquakes and their prediction mechanisms with different approaches, such as the source rupture process (Ma et al. 2001; Chen et al. 2012; Herring, 1998; He et al. 2012; Wang et al. 2010), geological structure (Chen et al.

2009; Zhang et al. 2011), deep structure (Zhu et al. 2008; Chen et al. 2012), and dynamic evolution. However, given a lack of information, some key causal factors of the two earthquakes have not been discovered. For example, why did the southern Longmenshan fault remain quiet during the Wenchuan earthquake occurrence in the northern segment of the fault? Why did the latter segment remain quiet over a five year span during which the Lushan earthquake occurred in the southern segment? What is the relationship between these earthquakes?

This paper provides some evidence regarding the above questions to researchers by using data from multi-source remote sensing, seismicity, and GPS monitoring of crustal movement. Further, we examine the southern segment of the LFZ using an updated structural geologic interpretation of the region.

1 Study Area and Methodology

The study area (Figure 1) is in the southern section of the LFZ and is between 102°E and 104°E, 29.5°N and 31°N. It covers south of the Longmenshan fault and the entire area of the Lushan earthquake.

According to information released by the China Earthquake Networks Center, the epicenter of the Lushan earthquake was at 30.3°N and 103°E with depth 13 km. This location is just within the southern section of the LFZ, and is at the junction of the Nanbaoshan syncline of the Sichuan Basin and Lushan synclinal (Figure 1). The Nanbaoshan and Lushan synclinal folds consist of Cretaceous Cenozoic systems. The epicenter was also to the east of the Shuangshi and Pengguan faults, at distances about 1.5–10.5 km from those faults. The epi-center is within the footwall of former fault.

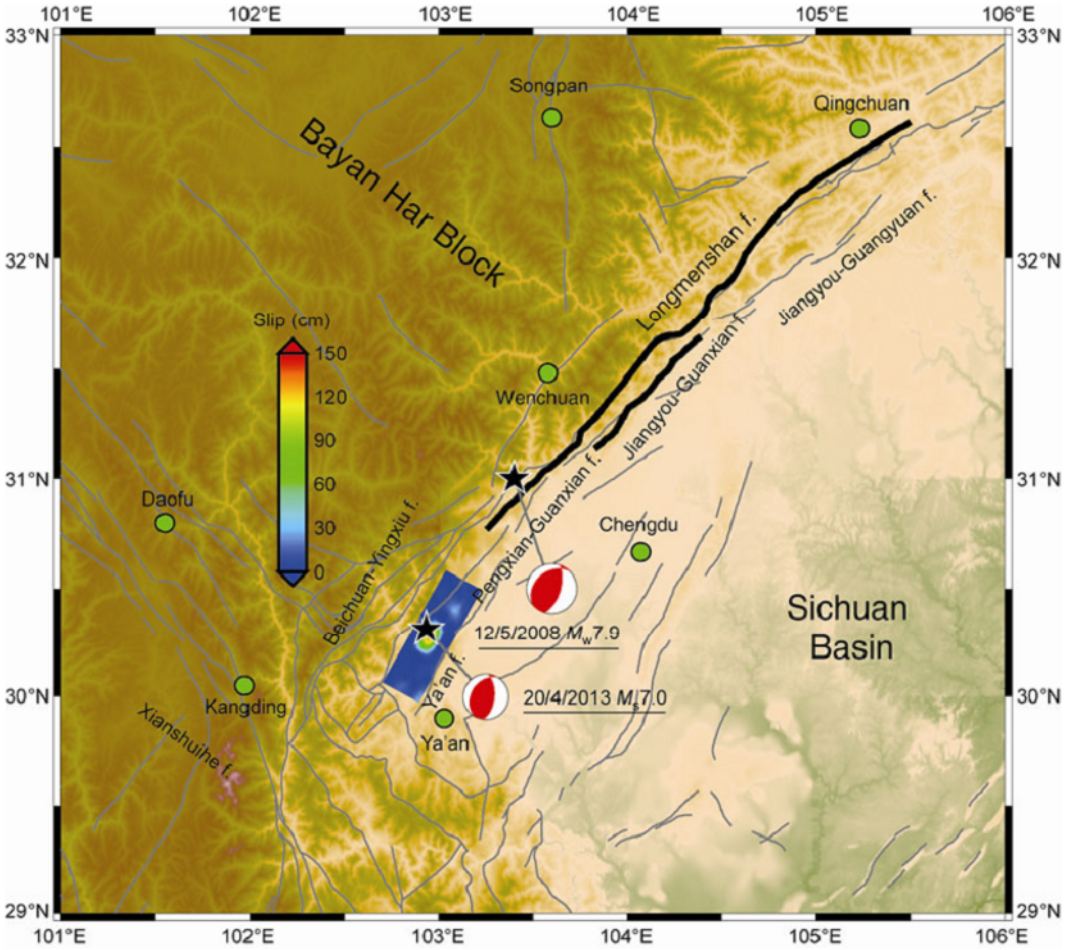

Figure 1 Study area and tectonic map of Lushan region and surroundings. Gray lines represent faults. Solid red polygons represent focal mechanisms of 2008 M_s 7.9 Wenchuan and 2013 M_s 7.0 Lushan earthquakes. Green circles represent principal cities and counties (Shan et al. 2013).

We used various data to extract and analyze the fault zone. These were multi-source remote sensing data (Landsat-5, Landsat-7, SPOT-4, SPOT-5, RADARSAT-2, and GPS movement monitoring) and topography data from the Shuttle Radar Topography Mission (SRTM) to generate a DEM (Pirasteh et al. 2009) (Table 1).

Table 1 Datasets used in the study

Data	Period	Description
Landsat-7	2000-05-20	Spatial resolution 30/15 m, swath width 185 km
SPOT-5	2006-06-03	Spatial resolution 10/5 m, swath width 60 km
SPOT-4	2011-04-09	Spatial resolution 20/10 m, swath width 60 km
RADARSAT-2	2012-03-04	Spatial resolution 30 m, nominal swath width 150 km
GPS data	1998–2004	Crustal Movement Observation Network of China (Gan et al 2007)
Epicenter	Last 100 years	Chengdu Earthquake Mitigation Bureau
SRTM-DEM	2000	Spatial resolution 30 m
Geologic structure	2004	China Geological Survey Bureau

Three major steps were executed to determine relationships between structural features and earthquakes (Figure 2).

Digital image processing was applied to satellite images (Figure 3) in order to extract the structural features, using ENVI software. Those images were geometrically corrected using a new approach called a polynomial correction model (Figure 2).

In order to extract objects, visual and digital onscreen interpretation was done for both satellite images and the SRTM DEM. A Laplacian convolution filter (Pirasteh et al. 2009; Pirasteh et al. 2011) was applied to the images to enhance structural features. Photographic and geotechnical elements such as tone, shape, drainage and linearity were the major clues for identifying image structural features. Objects were compared with the 2004 geological map of China from the China Geological Survey Bureau. Information from the ground truth samples (Figure 4) were compared with that map. In addition, information extracted from the satellite images and DEM were verified with the

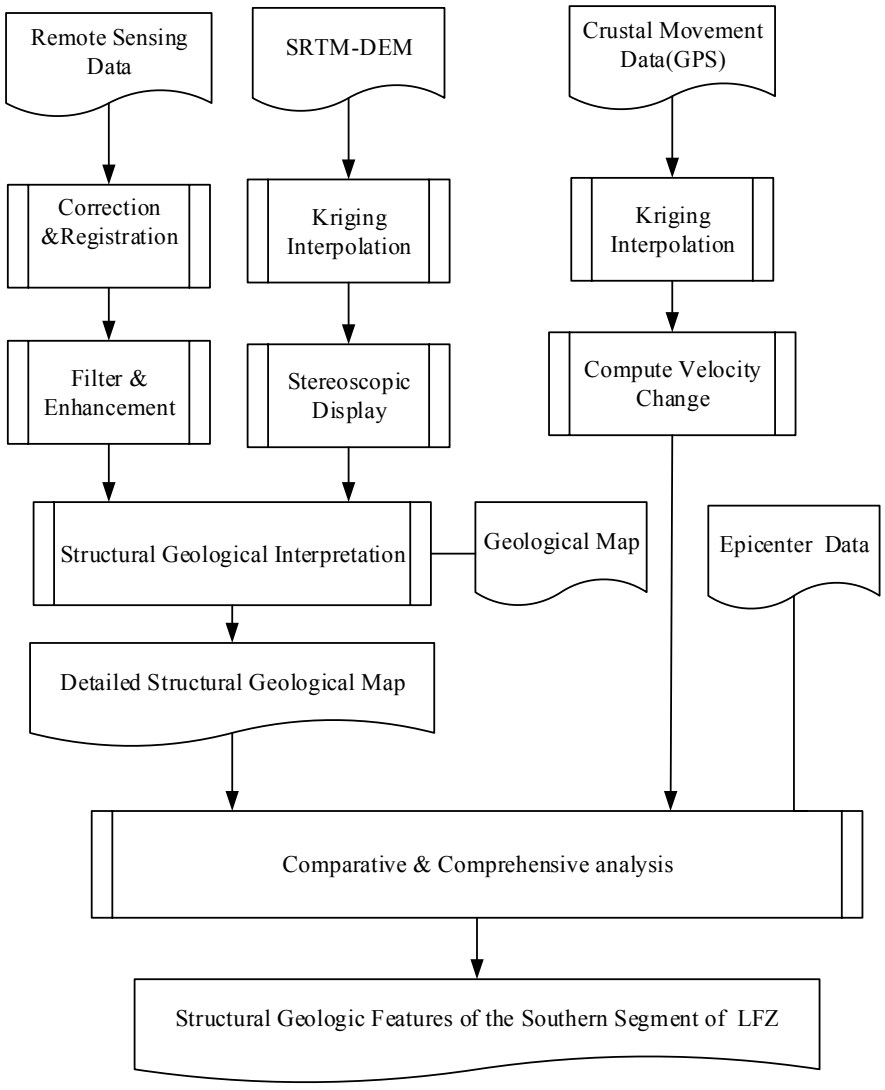

Figure 2 Flowchart of research work.

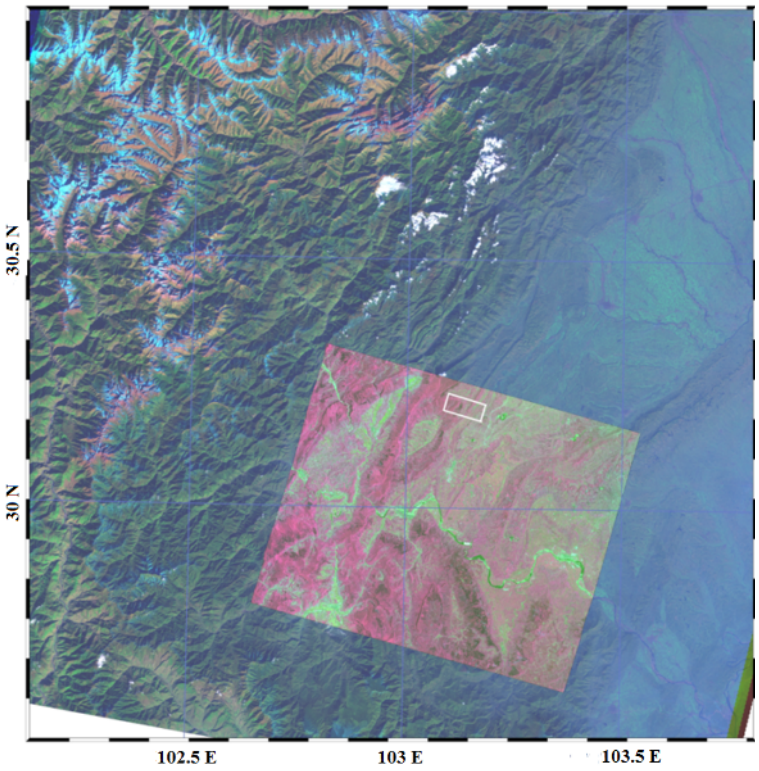

Figure 3 ETM and SPOT images of study area (entire image is ETM (3-2-1 bands synthetic) image superimposed on SPOT5 (4-3-2 bands synthetic)). White rectangle shows area of sample collection.

Figure 4 Road damage caused by earthquake in the southern segment of Longmenshan fault zone (LFZ). The photo was taken in Baoxing Country Daxi Town Caojia Village (E 102.80° N30.18°), Southwest China.

ground truth samples and geological map to validate the accuracy of the research. Further, crustal movement data using GPS were input to Surfer software to extract and analyze the first derivative difference and compare it to velocity change (Figure 5).

In the following section, we give the details of geometric correction and crustal movement.

1.1 Geometric Correction

A recorded image from a satellite or airborne sensor contains serious geometric distortion. There are many factors related to geometric error, e.g., earth's rotation and curvature, platform height, attitude, velocity change and sensor operation. Two types of technology can be used for correcting two types of geometric distortion: A) Building a model of the distortion with source characteristics and size, and using this model to generate correction equations; B) correcting the distortion using relationships between map pixel location and its surface coordinates, although the analyst does not know the source of distortion and distortion type. Method B can also be used to correct image geometric distortion. As to the current situation, the sensor position and attitude measurement, accuracy is not very high. Distorted images still have many errors. This work used a polynomial correction model for geometric correction, building the relationship between image coordinates (x, y) and a reference coordinate system (X, Y) using

$$x = \sum_{i=0}^{N}\sum_{j=0}^{N-i} a_{ij} X^i Y^j$$
$$y = \sum_{i=0}^{N}\sum_{j=0}^{N-i} b_{ij} X^i Y^j \quad (1)$$

where, a_{ij} is a polynomial coefficient and N is the degree of the polynomial. The choice of N depends on the degree of image distortion, number of ground control points and magnitude of terrain displacement. Generally, if N = 6, one can correct image distortion, tilt, rotation and obtains good accuracy. When N is determined, root mean square (RMS) error of every ground control point can be calculated by

$$RMS_{error} = \sqrt{(x'-x)^2 + (y'-y)^2} \quad (2)$$

where (x, y) specifies the coordinates of ground

control points in the original image, and (x', y') designates control point coordinates from the polynomial calculation.

1.2 Orthographic correction

Orthographic correction can correct image point displacement produced by topographic relief and sensor error. This correction was done with the aid of the DEM. We used SRTM data with spatial resolution 30 m. The correction model selects the rational function model to change image coordinates (r, c) into spatial coordinates (X, Y, Z) (Equation 3).

$$\begin{cases} r = \dfrac{P_1(X, Y, Z)}{P_2(X, Y, Z)} \\ c = \dfrac{P_3(X, Y, Z)}{P_4(X, Y, Z)} \end{cases} \quad (3)$$

1.3 GPS Data Processing

GPS data from 1998 to 2004 were collected from the crustal movement observation network of China. This network includes 27 continuous stations, 55 annual observation campaign stations with occupation duration 7 days for each survey, and 1000 campaign stations with observations from 1999, 2001 and 2004 with occupation duration at least 4 days for each survey (Gan and Zhang 2007). The data were processed in five steps (Shen et al. 2001): (1) All observation data for a given day were combined to solve daily loosely constrained station coordinates and satellite orbits using GAMIT software (King and Bock 1995); (2) daily solution at local stations was combined with loosely constrained global solutions of the 80 IGS core using GLOBK software (Herring 1998) and tracking stations of the Scripps Orbital and Position Analysis Center (SOPAC, http://sopac.ucsd.edu/); (3) station positions and velocities were estimated in the ITRF2000 reference frame using QOCA software (Dong et al. 1998). QOCA modeling of the data was done through sequential Kalman filtering that allowed adjustment for global translation and rotation of each daily solution; (4) the velocity solution was transformed into a Eurasia-fixed reference frame using the Euler vector of Eurasia with respect to the ITRF2000, deduced from 10 IGS stations (NYA L, ONSA, HERS, W SRT, KOSG, WTZR, VILL, GLSV, I RKT, and TIXI) in the stable Eurasia; (5) interpolation using a kriging algorithm (Isaaks and Srivastava 1989). To obtain crustal field data for the study area, GPS vector data were decomposed into east and south. Then, they were interpolated independently. South and east direction vectors were synthesized into one vector. The kriging search neighborhood was defined as oval. To have sufficient sample points, major axis distance was set to 5° and minor axis distance to 3°.

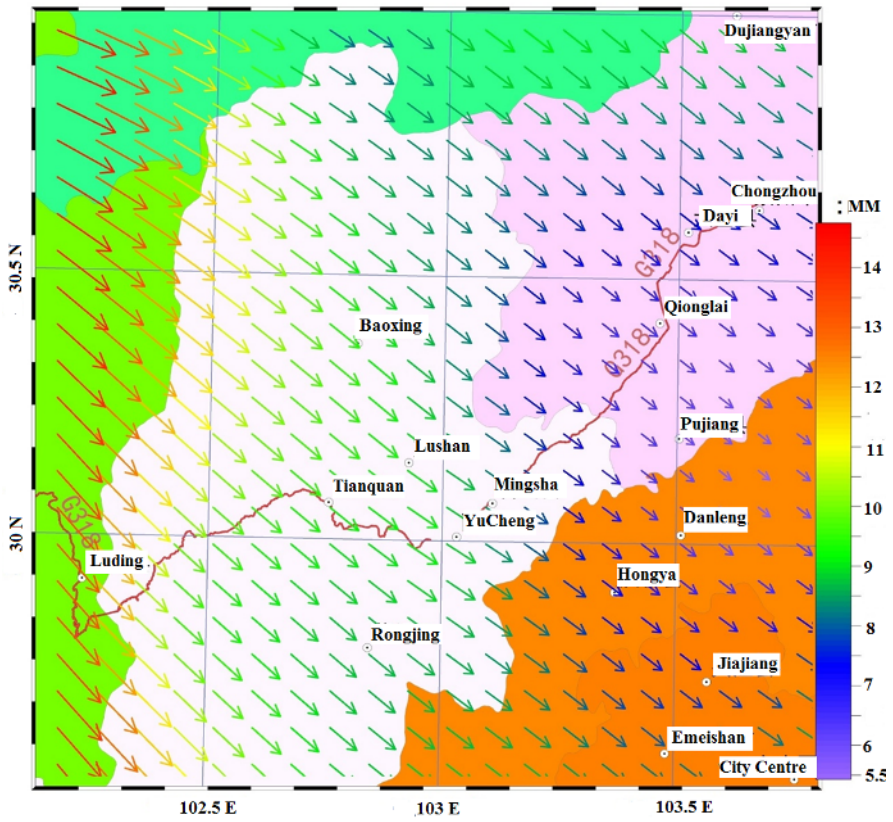

Figure 5 Crustal movement velocity distribution data from Crustal Movement Observation Network of China, interpolated by kriging algorithm. Length and color of arrows indicates motion velocity. Black labels indicate Chinese administrative divisions.

2 Results and Discussion

2.1 Recognition of fault zone

Remote sensing images record and reflect the surface aspect of spectrum and space information. In terms of rock distribution area, there are many differences in rock mineral composition, physicochemical properties, contrast hue, texture, geomorphology, drainage and vegetation, and differences should be consistent with the rock distribution boundaries.

Normally, to identify a rock type from space, four stages must be used. In our study area, the stripe (i.e., stratigraphic unit), stripes and tonal (i.e. multiple stratigraphic units) show image differences that are produced by different rock types (Figure 3). During fault and lineament identification (Ali et al. 2003; Ali and Pirasteh 2004), principles of structural geology were considered. Normally, lineaments on a satellite image are identified by distinct linearity and difference of tone. Drainage patterns are defined by lineament features. Also, linearity of vegetation can be an effective indication of faults and lineaments. A human-computer vision method was used to interpret unique structural features evident in the study area. A sharp line with strong linearity is a powerful signature to identify fault zones (Figure 6) on images. Basically, this signature is interpreted by image elements and remote sensing techniques for recognizing stratigraphic units. Our investigation showed that image edge change, statistical indicators of image area, topography, geomorphology, epicenter data distribution, and earth crust motion data are significant elements for interpreting structural geology from space and its influence on the Wenchuan and Lushan earthquakes (Joshi et al. 2013; Kaya and Muftuoglu 2004; Walker 2006).

The satellite images were digitally processed and structural geologic features extracted. Stretching and edge enhancement (2% linear stretch processing) techniques in ENVI software showed agreement with existing structural features in a geological map of the area. However, because of the Wenchuan and Lushan earthquakes, large big ruptures have been generated (Figure 7). These are easily detectable using high resolution remote sensing techniques.

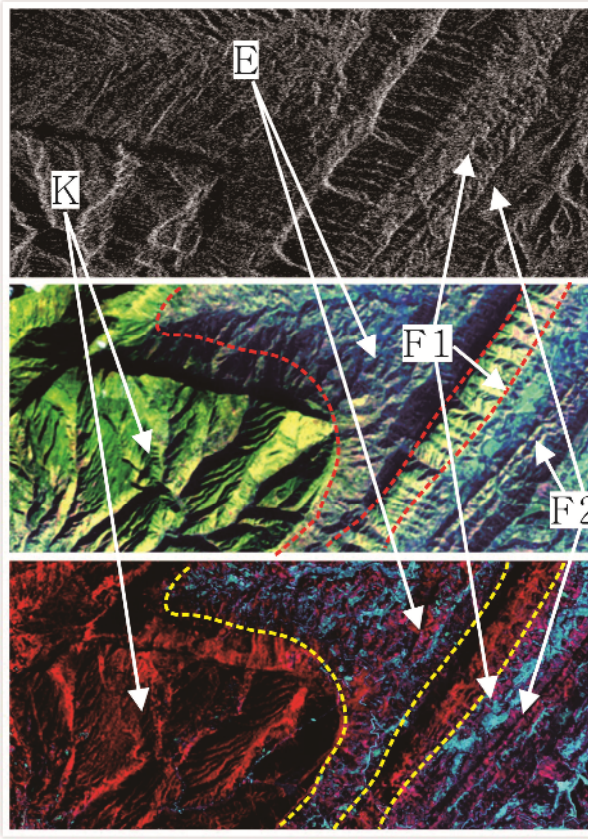

Figure 6 Remote sensing stratigraphy and fault zones in northwest of Ya'an, Sichuan, China: RADARSAT-2 SAR image (top), Landsat-7 FCC 542 band composite image (middle), SPOT-5 FCC 432 band composite image (bottom).

Figure 7 Sandblast body alignment from ground fissure caused by earthquake (left photo). Trench for research of southern segment of LFZ (right photo).

Compiling the geological map of the study area with the satellite images, we could determine whether intersection relationships between the Cretaceous (K) and early Tertiary (E) periods (Figure 6) had a considerable effect on earthquake occurrence. Both of the strata have a clear demarcation (dotted line in the figure) and alternate with each other. Cretaceous strata rocks are outcropped. Weathering resistance is strong across the study area, with a stable distribution. Vegetation growth is poorer than in the Tertiary period. Fault tracks (F1 and F2; Figure 6) are clear and extend northeastward. This is a thrust fault with no obvious strike-slip traces. According to the old and new relationships of strata, we infer that fault F1 is earlier than F2.

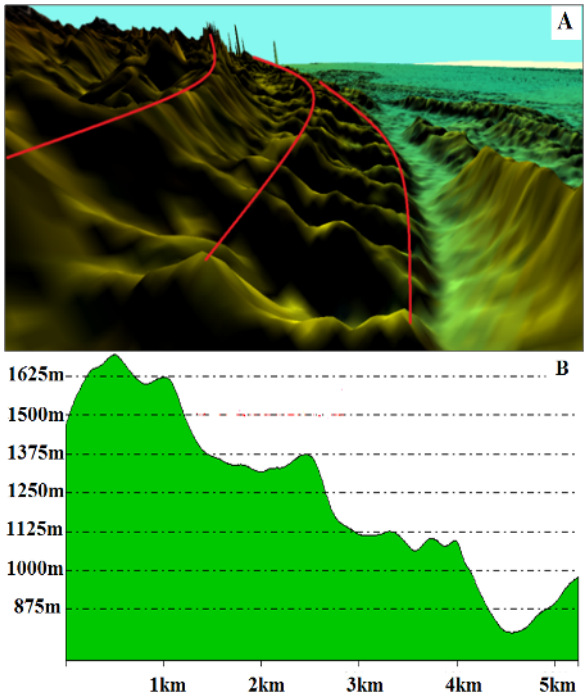

Figure 8 (A) Terrain caused by multistage abdominal thrust tectonic movement in Longmenshan front fault zone and (B) terrain profile.

A three-dimensional display based on the SRTM DEM (Figure 8A) shows a multi-stepped topography (red line) caused by multi-period earthquake activity in the region and its effects. This also shows that the region is very seismically active and prone to future earthquakes of high intensity and magnitude. Figure 8B depicts an east-west cross-section, which shows ground elevation changes caused by the recent earthquakes. Both the DEM and terrain profile help to interpret active faults in the study area.

2.2 Fault Zone Distribution

Within the study area, fault structure is formed by compression in the abdomen tectonic movement. Lineaments extend from northeast to northwest and the two main faults are nearly 90° from northeast through southwest. The entire area is controlled by the Songpan-Ganzi, Tibet, and Yangtze plates and has a typical nappe structure, with northeast- and southwest-trending strike slips. There are major features such as the Longmenshan fault zone, which consists of the Wenmao, Jintang and Beimushan faults. They are located from 102.5°E to 103°E, with north through east and north through west trends. Field observation indicate that the central fault belt –Beichuan-Yingxiu fault zone has been continued. However, remotely sensed data reveals that this feature has not been continued or is probably absent in the imagery, especially at 103.15°E where there is a 5-km segment missing.

Thus, we infer that the existing fault zone has been formed by several tectonic movements in the region. The central fault and back range fault zone trend from north to south and merge with each other. Trends of the mountain front (Dujiangyan-Hanwang) fault and central fault have maintained their consistency. Distances between them exceed 20 km, with an altitude difference of 3 km. This reveals that the two fault zones are relatively independent and the time of tectonic movement is well into the future. The number of secondary faults of the front fault gradually increases from north to south, reaching more than ten. The two faults show a symmetric distribution with average intervening distance < 3 km. They have caused a tectonic rift basin in Lushan County area. The southern fracture of State Highway 318 is toward the north through west trending fault. The rupture length of the secondary fault is less than those of the north through east trending fractures (Figure 9).

2.3 Fault zone activity features

The earth crustal movement data and map (Figure 10A) show that the crustal movement direction is essentially uniform across the study area. This direction reflects a weak chronological deflection from north to south with average speed

~8 mm/year. In addition, the velocity of motion is asymmetric. Thus, the area is a typical variable-speed and stress concentration belt. The region's highest movement speed is > 14.5 mm/year, which is located west of the back mountain fault and near the Daduhe fault zone. The minimum velocity of motion is in the northeast part of the city of Meishan City DanLeng Country, with momentum < 5.5 mm/year. A typical structure of the study area with a strong crustal activity belt is evident there. There is also an inflection point there (Figure 11) of variable speed. From the moving velocity profile (Figure 10C), the epicenter of the M_s 8 Wenchuan earthquake and M_s 7 Lushan earthquake belongs to the later one. The former fault contains the back mountain fault zone of the Longmenshan, Daduhe and Beimushan fault zones. The angle of movement direction and fault zone relationships reveal that the back mountain fault and north fracture section of the center fault have a clockwise rotation trend. The back mountain fracture rotated more than the central fracture. The front fault is vertical, and the movement direction and strike-slip trend was verified to be less than the central fracture. The south section of the central (Jintang) fault and west section of the Beimushan fault have a strong counterclockwise rotation trend. Finally, the study area has experienced ten independent earthquakes of > M_s 5.0 in the last 100 years and four of > M_s 6.0. The latter are the Wenchuan and Lushan earthquakes, plus the 1941 Baoxing (30.4°N, 102.2°E) and 1970 Dayi quakes.

The earth crust movement data indicate that the crustal movement direction in study area is essentially uniform. There has been no earthquake in the area 30°N–30°15′N, which is between the Wenchuan and Lushan

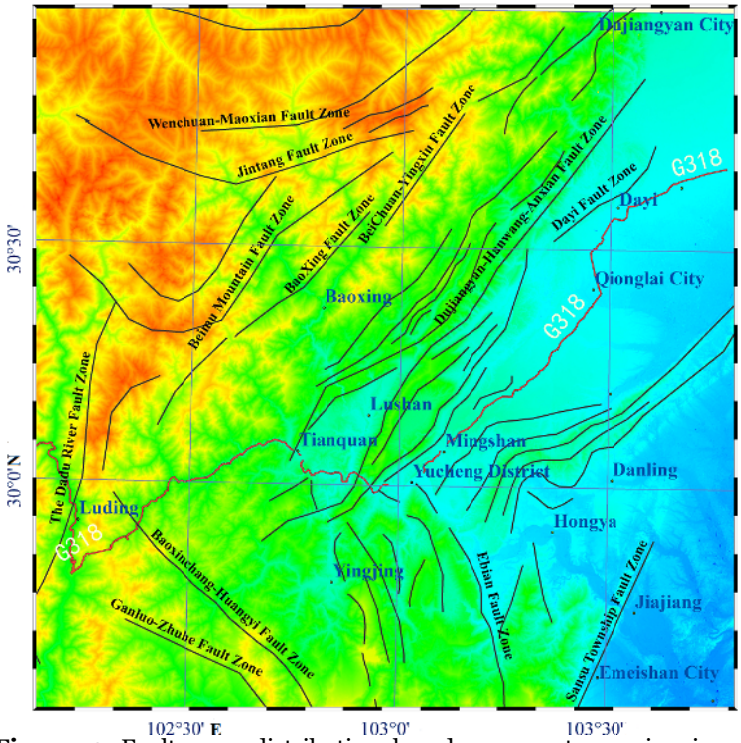

Figure 9 Fault zone distribution based on remote sensing image recognition.

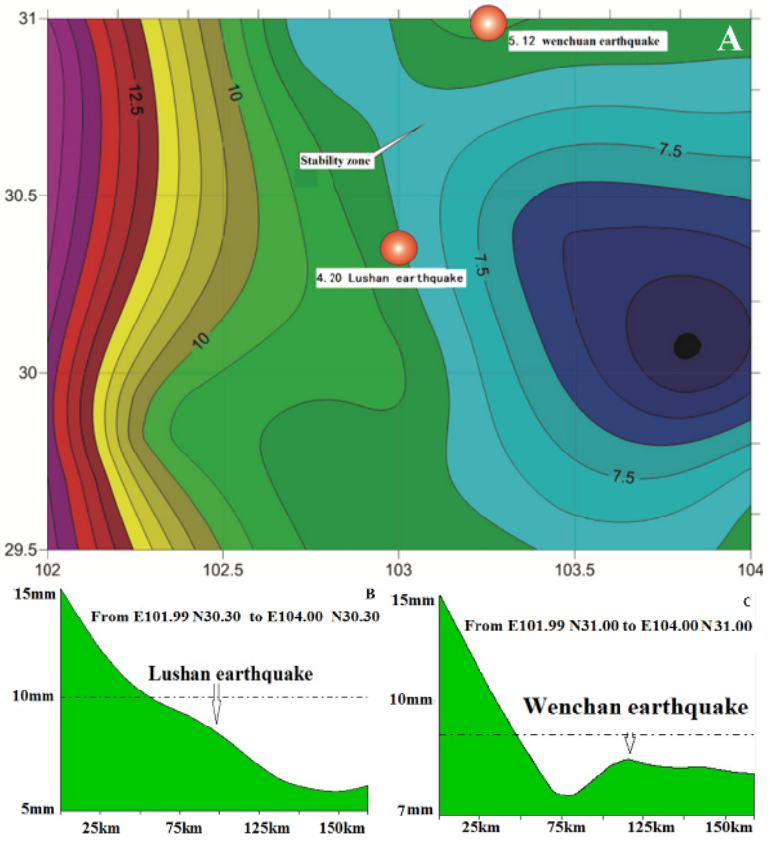

Figure 10 (A) Crustal movement velocity contour map; (B, C) Velocity profile (Unit is mm/year).

epicenters.

In contrast with the movement speed (Figure 10B), there is a nearly constant belt of northwest trend in the Songpan-Ganzi block, with 20-km width and trends from the northeast to the front fault zone (the junction of the Songpan-Ganzi and Yangtze plates). However, there is likely little potential of earthquakes in this area. This evidence combined with the fault zone distribution (Figure 11) demonstrate that the Lushan earthquake was not an aftershock of the Wenchuan earthquake. The epicenter distribution plus crustal movement speed and spatial distribution analysis of the fault zone in the linear region at 30°N with northwest trends reveal a typical multidirectional shear zone. Trends in this area are NE and NW. The crustal movement speed decreases sharply and stress accumulates rapidly. This is also a strong tectonically active belt with evidence of stretch-draw and squeezing effects.

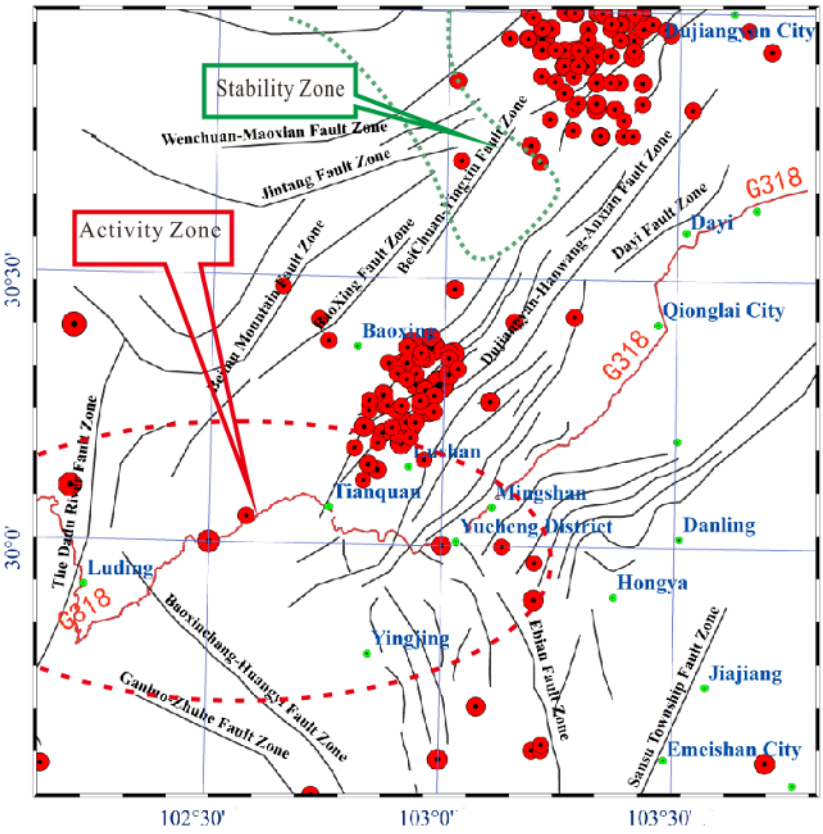

Figure 11 Distribution of fault zones and epicenter.

3 Conclusions

This paper identified faults in the study area based on remote sensing data and a DEM. After combining the regional crustal velocity field with epicenter distribution data, we conclude that the M_s 8 Wenchuan and M_s 7 Lushan earthquakes occurred on two relatively independent faults. There is a nearly constant motion speed area between these two faults, with a slow stress change rate. The central fault and back fault gradually merged from north to south. Trends were transferred and their distance increased from the central fault to the front back fault. The fault zones present a complex intersection relationship in the 30–50 km range on both sides of State Highway 318. There is also a strong multi-directional shear belt with potential for an earthquake. In the medium to long term, activity there is anticipated to be more intense than in the northern study area.

Acknowledgements

The study was funded by the National Natural Science Foundation of China (Grant No. 41001253), Chinese Postdoctoral Science Foundation (Grant No. 2012M521717), and National Science and Technology Major Project (Grant No. 03-Y30B06-9001-13/15). The authors thank Beijing SPOT Image Ltd. for providing SPOT4, SPOT5 and RadarSat-2 remote sensing images. Special thanks go to the China Crustal Movement Observation Network for providing GPS data. The authors appreciate WEN Xue-ze, YI Fei, LIU Hao, DING Zhi-ming and REN Yu for their knowledge contributions.

References

Ali SA, Pirasteh S (2004) Geological applications of Landsat Enhanced Thematic Mapper (ETM) data and Geographic Information System (GIS). International journal of remote sensing 25 (21): 4715-4727. DOI: 10.1080/01431160410001688295

Ali SA, Pirasteh S (2003) Remote Sensing and GIS Study of Tectonics and Net Erosion Rates in the Zagros Structural Belt, Southwestern Iran. Gisciences and Remote Sensing Journal 40 (4): 253-262. DOI: 10.2747/0749-3878.40.4.258

Chen JH, Liu QY, Li SC (2009) Seismotectonic study by relocation of the Wenchuan MS 8.0 earthquake sequence. Chinese Journal of Geophysics 52 (2): 390-397.

Chen QC, Feng CJ, Meng W(2012) Analysis of in situ stress measurements at the northeastern section of the Longmenshan fault zone after the 5.12 Wenchuan Earthquake. Chinese Journal of Geophysics Chinese Edition 55 (12): 923-3932. DOI: 10.6038/j.issn.0001-5733.2012.12.005

Cui P, Wei FQ, He SM (2008) Mountain Disasters Induced by the Earthquake of May 12 in Wenchuan and the Disasters Mitigation. Journal of Mountain Science 26(3): 280-282. (In Chinese)

Ehrlich D, Guo HD, Molch K (2009) Identifying damage caused by the 2008 Wenchuan earthquake from VHR remote sensing data. International Journal of Digital Earth 2(4): 309-326. DOI: 10.1080/17538940902767401

Dong D, Herring T, King R (1998) Estimating regional deformation from a combination of space and terrestrial geodetic data. Journal of Geodesy 72(4): 200-214. DOI: 10.1007/s001900050161

Isaaks E. H., Srivastava R. M.(1989) An Introduction to Applied Geostatistics. Oxford University Press, USA. p105. DOI: 10.2307/1269430

Farrokhnia A R, Pirasteh S, Pourkermani M, et al. (2011) Geo-Information technology for mass wasting hazard zonation: Central-west Alborz Iran. Disaster Advances Journal 4(3): 24-33. DOI: 10.1007/s12517-010-0238-7

Gan WP, Zhang ZK (2007) Present-day crustal motion within the Tibetan Plateau inferred from GPS measurements. J Geophys Res 112 B08416. DOI: 10.1029/2005JB004120

Herring T (1998) GLOBK: Global Kalman filter VLBI and GPS analysis program, v 4.1. Mass. Inst. of Technol, Cambridge. p54. Available on: http://www-gpsg.mit.edu/~simon/gtgk/GLOBK_Ref.pdf (Accessed on 10 Feb 2010)

He ZT, Ma BQ, Li YS (2012) Width and Hanging Wall Effect of Surface Rupture Caused by Wenchuan Earthquake. Acta Scientiarum Naturalium Universitatis Pekinensis 48(6): 886-894. DOI: 10.13209/j.0479-8023.2012.115

Joshi P N, Maurya D M, Chamyal L S (2013) Morphotectonic segmentation and spatial variability of neotectonic activity along the Narmada Son Fault, Western India: Remote sensing and GIS analysis. Geomorphology 180: 292-306. DOI: 10.1016/j.geomorph.2012.10.023

Li CC, Yong KR, Hu W, et al. (2013) The Lushan M_S7.0 earthquake and activity of the southern segment of the Longmenshan fault zone. Chinese Science Bulletin 58(29): 3475-3482. DOI: 10.1007/s11434-013-6009-6

Liu GX, Li J, Xu Z (2010) Surface deformation associated with the 2008 Ms8.0 Wenchuan earthquake from ALOS L-band SAR interferometry. International Journal of Applied Earth Observation and Geoinformation 12(6): 496-505. DOI: 10.1016/j.jag.2010.05.005.

Li Y, Zhou RJ (2006) The geology of the eastern margin of the Qinghai-Tibet plateau. Geological publishing house, Beijing, China. pp 182.

Ma ZJ, Zhang JS, Wang YP (2001) Changes of the 3-d movement sense along with time in the Qinghai-Xizang plateau. In: Study on the recent deformation and dynamics of the lithosphere of Qinghai-Xizang plateau. Seismological Press, Beijing, China. pp 88-105.

Pei JL, Li HB, Wang H, et al. (2014) Magnetic properties of the Wenchuan Earthquake Fault Scientific Drilling Project Hole-1 (WFSD-1), Sichuan Province, China. Earth Planets and Space 66: 23. DOI: 10.1186/1880-5981-66-23

Saied P, Amir M, Alam M (2008) Integration of geo information technology and survey analysis for development in mitigation study against earthquake: a case study for Esfahan Iran. Disaster Advances 1(3): 20-26.

Saied P, Biswajeet P, Amir M (2009) Stability Mapping and Landslide Recognition in Zagros Mountain South West Iran: A Case Study. Disaster Advances 2(1): 47-53.

Pirasteh S, Pradhan B, Safari HO (2011) Coupling of DEM and remote sensing based approaches for semi-automated detection of regional geo-structural features in Zagros Mountain, Iran. Arabian Journal of Geosciences 6(1): 91-99. DOI: 10.1007/s12517-011-0361-0

Saied P, Ali SA (2005) lithostratigraphical study from Dezful to Brojerd-Dorood areas SW Iran using digital topography, remote sensing and GIS. Indian petroleum geology journal 13 (1): 1-13.

King R, Bock Y (1995) Documentation of the GAMIT GPS analysis software, version 9.3. Mass. Inst. of Technol, Cambridge, p67. Available on: http://www-gpsg.mit.edu/~simon/gtgk/ GAMIT.pdf (Accessed on 5 Mar 2013)

Shan B, Xiong X, Zheng Y (2013) Stress changes on major faults caused by 2013 Lushan earthquake and its relationship with 2008 Wenchuan earthquake. Science China 56(7): 1169-1176. DOI: 10.1007/s11430-013-4642-1

Shen, ZK, Wang M, Li Y, et al. (2001) Crustal deformation along the Altyn Tagh fault system, western China, from GPS. JOURNAL OF GEOPHYSICAL RESEARCH-SOLID EARTH 106(B12): 30607-30621. DOI: 10.1029/2001JB000349

Kaya S, Muftuoglu O (2004) Racing the geometry of an active fault using remote sensing and digital elevation model: Ganos segment, North Anatolian Fault zone, Turkey. International Journal of Remote Sensing 25(19): 3843-3855. DOI: 10.1080/01431160310001652394

Walker R. T. (2006) A remote sensing study of active folding and faulting in southern Kerman province, S.E. Iran. Journal of Structural Geology 8: 654-668. DOI: 10.1016/j.jsg.2005.12.014

Wang H, Ran YK, Chen LC (2010) The study of near-fault horizontal shortening of the surface rupture in Wenchuan Ms 8.0 earthquake. Earth Science Frontiers 5: 43-52.

Yi GX, Wen XZ, Xin H (2013) Stress state and major earthquake risk on the southern segment of the Longmenshan fault zone. Chinese Journal of Geophysics 6(4): 1112-1113. DOI: 10.6038/cjg20130407

Yuka Maekawa, Tetsuro Hirono, Hikaru Yabuta, et al. (2014) Estimation of slip parameters associated with frictional heating during the 1999 Taiwan Chi-Chi earthquake by vitrinite reflectance geothermometry. Earth Planets and Space 66:28. DOI: 10.1186/1880-5981-66-28

Zhang GG, Yang ZQ, Wang QL (2011) Inversion of Three Dimension Sliding Rate of Longmenshan Fault And Characters of Its Segments. Journal of Geodesy and Geodynamics 31(1): 31-54.

Zhu JS (2008) The Wenchuan earthquake occurrence background in deep structure and dynamics of lithosphere. Journal of Chengdu University of Technology 35(4): 348-356.